Architecture and growth history of a Miocene carbonate platform from 3D seismic reflection data; Luconia province, offshore Sarawak, Malaysia

Valentina Zampetti[a,*], Wolfgang Schlager[a], Jan-Henk van Konijnenburg[b], Arnout-Jan Everts[b]

[a]*Department of Sedimentology and Marine Geology, Faculty of Earth and Life Sciences, Vrije Universiteit, De Boelelaan 1085, Amsterdam 1081 The Netherlands*
[b]*Sarawak Shell Berhad, Sabah Shell Petroleum Co Ltd, Locked Bag No.1, 98009 Miri Sarawak, Malaysia*

Abstract

Using 3D seismic reflection data and wireline logs we reconstruct in detail the architecture and growth history of a Miocene carbonate platform in the Luconia province, offshore Sarawak, Malaysia. Platform growth started in the Late Oligocene to Early Miocene, by coalescence of isolated patch reefs. The growth history includes phases of progradation, backstepping and occasional collapsing of platform flanks, guided by syndepositional faulting. The most pronounced seismic reflections in the platform correspond to flooding events (thin transgressive systems tracts). Subaerial exposure preceding the flooding could be demonstrated in only one case. Platform growth was terminated by gradual submergence (drowning) indicated by smooth, concentric seismic reflectors forming a convex mound.
© 2004 Elsevier Ltd. All rights reserved.

Keywords: Carbonate platform; 3D seismics; Growth history

1. Introduction

During the Tertiary, deposition of tropical shallow-water carbonates, including reefs, was extensive in the tectonically complex region of Southeast Asia (Epting, 1989; Wilson, 2002). Miocene carbonates are widespread in the Luconia province, offshore Sarawak, Malaysia, where over 200 carbonate platforms ranging in size from a few to more than 200 km^2 have been mapped (Fig. 1). Despite the fact that the carbonate platforms in the Luconia province contain numerous gas reservoirs, little is published about their geological evolution, stratigraphy and chronostratigraphy (Bracco Gartner, 2000; Epting, 1980, 1989; Vahrenkamp, 1996, 1998).

Previous studies based on 2D seismic lines, core slabs and thin sections proposed rather different interpretations for the evolution and demise of carbonate platforms in the Luconia province (Epting, 1980, 1989; Vahrenkamp, 1996, 1998). In Central Luconia, carbonate deposition started during the Early Miocene, but was most prolific during the Middle to Late Miocene. While carbonate deposition continued in the northern part of the province, most of the platforms in the central and southern areas were buried by prograding marine deltaic siliciclastics (Aigner, Doyle, Lawrence, Epting & van Vliet., 1989; Epting, 1980, 1989).

Epting (1980, 1989) suggests that the overall architecture of the carbonate platforms is determined by four major processes, namely: (i) the rate of skeletal carbonate production, (ii) subsidence, (iii) relative sea-level fluctuation and (iv) the supply of clastic material from the Borneo deltas. Epting (1980, 1989) concluded that the termination of the platform was caused by sea-level rise that exceeded the rate of carbonate production (Fig. 2). Contrary to the drowning model proposed by Epting (1980, 1989) and Vahrenkamp (1996, 1998) indicates that sea-level lowering and subaerial exposure terminated the platform growth and that subaerial events also strongly influenced platform growth.

The aim of this study is to make a detailed reconstruction of depositional history of a Miocene carbonate platform in the Central Luconia Province. Using a recently acquired 3D seismic cube and wireline logs from three wells (Fig. 3), we

* Corresponding author. Tel.: +31-20-4447297; fax: +31-20-4449941.
E-mail address: valentina.zampetti@falw.vu.nl (V. Zampetti).
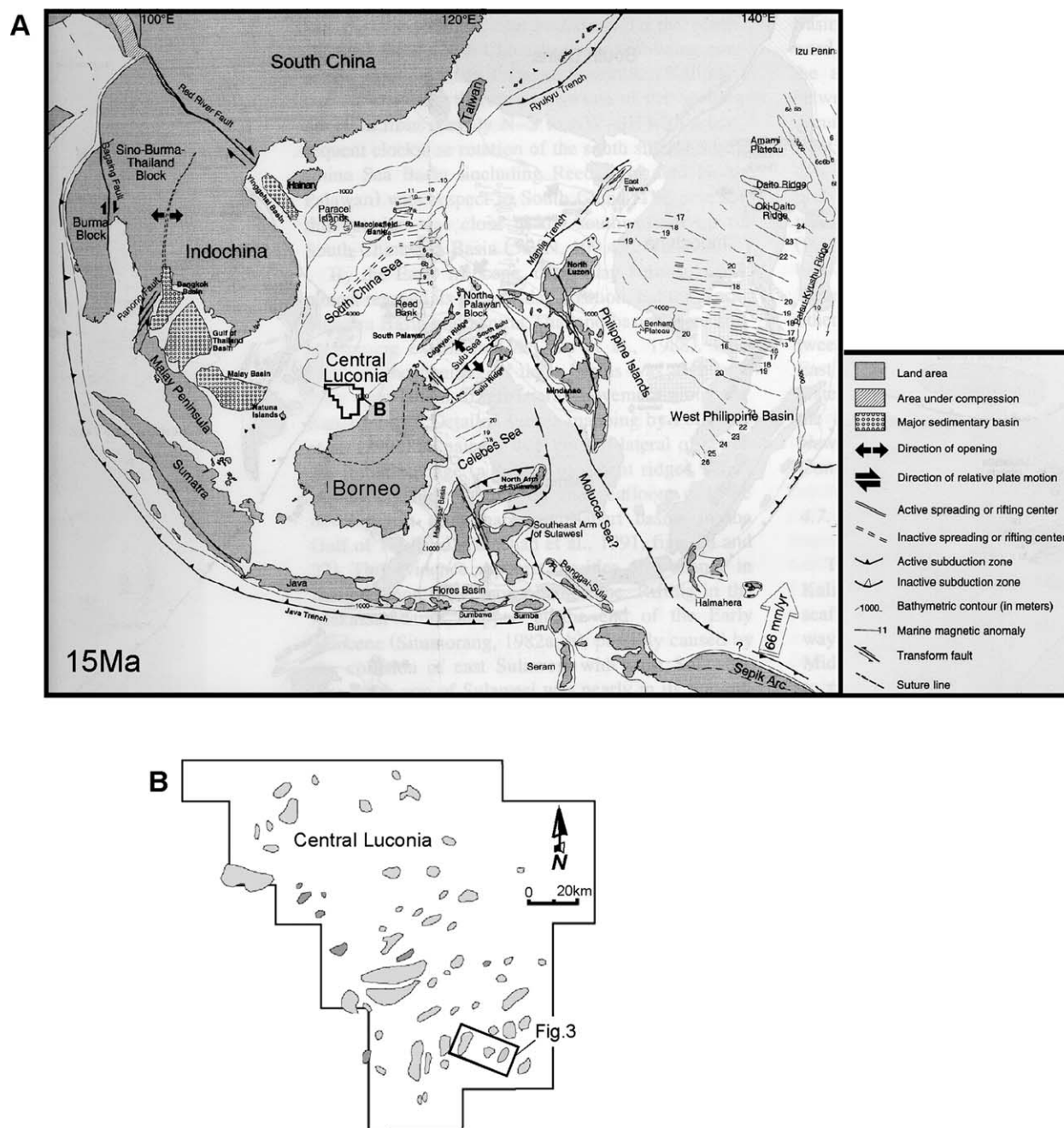
Fig. 1. (A) Mid-Miocene (15 Ma) reconstruction of SE Asia modified after Lee and Lawver (1995) and location of the Central Luconia Province. The southern part of the South China Sea is configured approximately as it is now. The Luconia Province (black box) is attached to northern Borneo, which is not rotated. (B) Distribution of the major carbonate platforms in Central Luconia (modified after Epting, 1980) and location of the 3D seismic survey used in this study.

propose a model for the evolution of the studied platform using detailed seismic evidence to better constrain geological processes affecting, controlling and modifying the evolution and demise of the platform.

2. Geological setting

The Luconia province is located in the South China Sea (Fig. 1). Structurally it is in an intermediate position between areas of extensive tectonic activity characterized by subsidence and faulting in the north and zones of pronounced Early to Mid Tertiary compressional tectonics in the south (Epting, 1980). At present it is a rather stable shelf of the island of Borneo (Fig. 1A). Its geological setting in the Oligocene and Miocene is not very well constrained. Some authors indicate that it was part of a NE-SW oriented shelf of Borneo (Lee & Lawver, 1995; Wilson & Moss, 1999). Other tectonic reconstructions assume that in the Oligocene the continental sliver of Luconia lay offshore
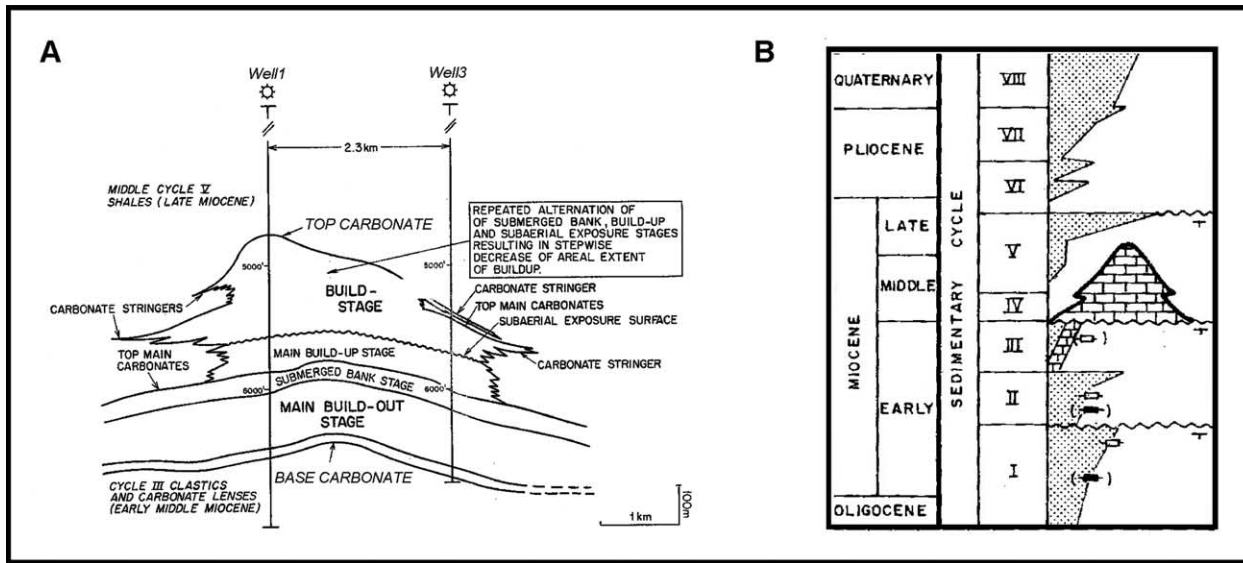
Fig. 2. (A) Growth history of an isolated carbonate platform in Luconia into stages reflecting variation in carbonate production, subsidence sea-level fluctuation and terrigenuos influx (Epting, 1989). (B) Depositional cycles identified in the carbonate platforms of the Luconia Province. Eight regressive sedimentary cycles are recognized in the Sarawak basin. In Central Luconia, carbonate deposition started during the Early Miocene (Cycle III), but was most prolific during the Middle to Late Miocene. Modified after Epting (1989).

Borneo and subsequently docked on to the microcontinent during the subduction and subsequent collision that formed the Rajang belt of northern Borneo (Hutchison, 1989; Taylor & Hayes, 1983). The recent paleogeographic reconstruction of Hall (1996) is not explicit about the Luconia Province. Implicitly, however, Hall's (1996) synthesis must also invoke a more offshore position as it

postulates destruction of a 500 km wide stretch of sea floor N of Borneo in the Middle and Late Miocene. Industry data (Doust, 1981; Epting, 1989) suggest that during the main phase of carbonate growth Luconia was already part of the continental margin of Borneo.

In spite of the different tectonic reconstructions for the Luconia Province, the Miocene platforms formed in
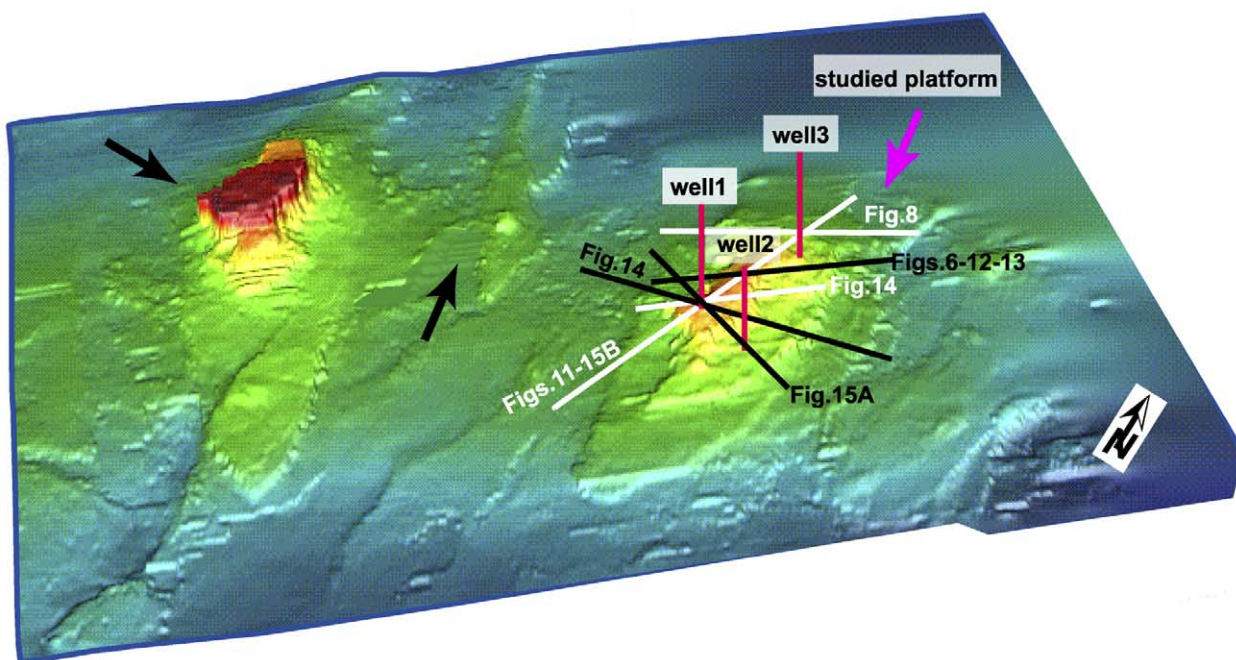

Fig. 3. 3D display of the seismic survey covering three isolated carbonate platforms (arrows). The studied platform (pink arrow), the location of the three wells and the seismic lines are shown. Location of the seismic survey shown in Fig. 1B.

V. Zampetti et al. / Marine and Petroleum Geology 21 (2004) 517–534

a tectonically more active setting than the present shelf. Regional cross-sections based on exploration seismics show that in the Early Miocene faulting and folding were widespread and that deformation activity decreased during Late Miocene and Pliocene (Doust, 1981; Epting, 1989).

3. Data and methods

The data made available by Petronas Nasional Berhad and Sarawak Shell Berhad include a 3D reflectivity volume, wireline logs from three vertical wells and core slabs and thin sections from two of the three vertical wells. The 3D seismic dataset contains 493 inlines and 1558 crosslines covering an approximate area of 200 km^2 and was loaded onto a Geoframe 3.7 workstation for interactive interpretation. Frequencies (instantaneous low frequency) range from a maximum value of 60 Hz in the overlying shale to 30 Hz in the carbonate platform with a depth resolution of 15 m (50 ft) and 40 m (130 ft), respectively. One well is located on the shallowest culmination of the platform, the other two along the platform flanks (Fig. 3). Well data

consist of sonic velocity, gamma ray, caliper and density logs as well as check-shot surveys.

Logs were correlated and tied to the 3D seismic data via synthetic seismograms (Fig. 4). Most reflections seen in a seismic section are composites of reflections from several interfaces. Synthetic seismograms provide a means of identifying reflections and determining which event relates to a particular interface or sequence of interfaces (Sheriff, 1977). To generate synthetics we used the Charisma Synthetic package (Geoframe, Schlumberger) and utilized both wavelet generation and wavelet extraction routine. In the wavelet generation routine (Fig. 4A and B) we chose a positive Ricker wavelet and applied frequencies ranging from 15 to 40 Hz to evaluate frequency effects. The wavelet generation routine allows the modeler to determine all parameters a priori. The wavelet extraction routine (Fig. 4C), on the other hand, estimates the wavelet from seismic based on a reflectivity curve and a reference seismic trace along the borehole (Fig. 4D) and takes into account not only a single frequency value but a range of them directly detected by the original seismic section and the filtering applied to it (Geoframe User's manual Schlumberger).
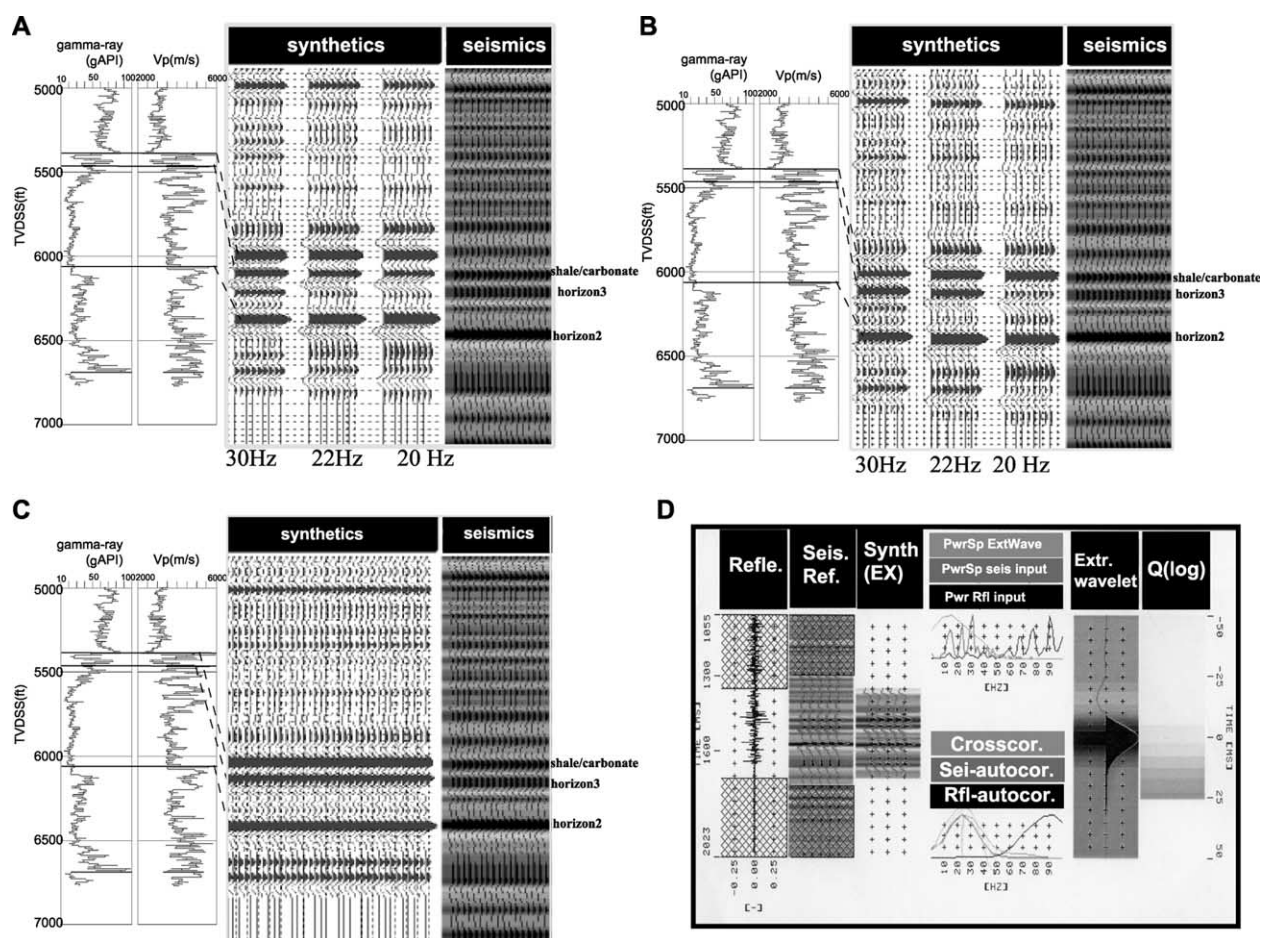

Fig. 4. Synthetics for well 3: (A) Using wavelet generation routine. Note good match in reflection character but persistent shift of reflection positions. (B) Same as (A) but with 95° shift. (C) Synthetic using wavelet extraction routine. Shift in phase is reduced between 20° and 30°. (D) Wavelet extraction panel showing the frequency range, the wavelet shape and the reflectivity log. Wavelet extraction was performed for an interval that brackets the shale-carbonate boundary.

Using the Charisma Volume attribute application, a variance cube was generated in time domain with a sample size of 16 bit, with orthogonal lines as neighbourhood definition and with a window of 11 samples (Geoframe User's Manual). Variance cube imaging essentially generates a cube of variance coefficients by calculating localized waveform similarity in both inline and crossline directions. The underlying assumption is that stratigraphic features are associated with definite seismic waveform expressions and that seismic traces cut by a fault generally have different seismic character than neighboring traces. Therefore a time slice from a variance cube would depict lineaments of high variance or low similarity (displayed in black) along faults and other features like reefs, slumps, channels, salt edges and unconformities.

Time-to-depth conversion for selected sections was carried out using Stratlog application in Charisma in order to identify 'time highs' that can represent just 'velocity pull-ups' and that would map out as a series of flat beds after

conversion in depth (e.g. horizon 2, see below). Even more time-to-depth converted sections were used to estimate slope angles and fault dips. Stratlog approach to depth conversion is to convert a 2D grid of time versus depth for the plane of the cross section using selected check-shot surveys at the specified cross section hinges. Points between the check-shot surveys are interpolated (Geoframe User's manual).

Core data and thin sections belong to the two wells located on the platform flanks (well 2 and well 3). Sedimentary logs of the two wells are subdivided by lithology and texture (Fig. 5; Bracco Gartner, 2000).

4. Seismic stratigraphic units

Four seismic stratigraphic units (A–D) are recognized within the studied carbonate platform (Fig. 6 and Table 1). A seismic unit is defined as a mapable interval of seismic reflections bounded by marker reflectors. The markers often coincide with distinct changes at the outer boundaries of the platform. The markers were labeled from bottom to top 'horizon 1' to 'horizon 4'. An extra marker labeled 'shale/carbonate' is not a stratigraphic horizon but shows the carbonate to shale boundary. Independently of the platform stratigraphy, we established a stratigraphy in the basin by tracing continuous reflectors in the shales. These reflectors are labelled from bottom to top 'shale 1' to 'shale 6' and correlated across the faults and slides of the platform flanks (see below).

Unit A is bounded by horizon 1 at its base and horizon 2 at its top. The unit has a maximum thickness of 70 ms (TWT) and it is characterized by low-amplitude discontinuous mound-shaped reflections just above horizon 1. Horizon 1 is essentially flat after depth migration showing no platform-basin differentiation.

On the western side horizon 2 makes a backwards step of about 50 ms. This step is interpreted as a primary platform margin, onlapped by a sediment wedge (Fig. 6). Time slices clearly display the evolution of this margin from a straight (fault-controlled) trend to the development of two concave structures as initial phase of backstepping (Fig. 7). The geometry of the eastern margin of unit A is disturbed by faulting that disrupts both the bounding reflections (horizon 1 and horizon 2) and the internal reflections. However, the northern part of the platform shows that the backstepped margin is also present on the eastern and western flanks (Fig. 8A). In these sections the thickness of the overlying carbonate deposits is reduced, the pull-up effect is small and the geometrical features of the horizons can be better observed. In particular horizon 2 is flat under the platform edifice but shows short, steep slopes on both flanks that dip away from the platform and remain unchanged after depth migration.

Unit B, bounded by horizon 2 and horizon 3, is about 68 ms (TWT) thick. This unit is only aggrading. There is no evidence of progradation. Unit B is characterized by low-amplitude internal reflections generally parallel to horizon 2 and affected by faulting, particularly near the platform margin.
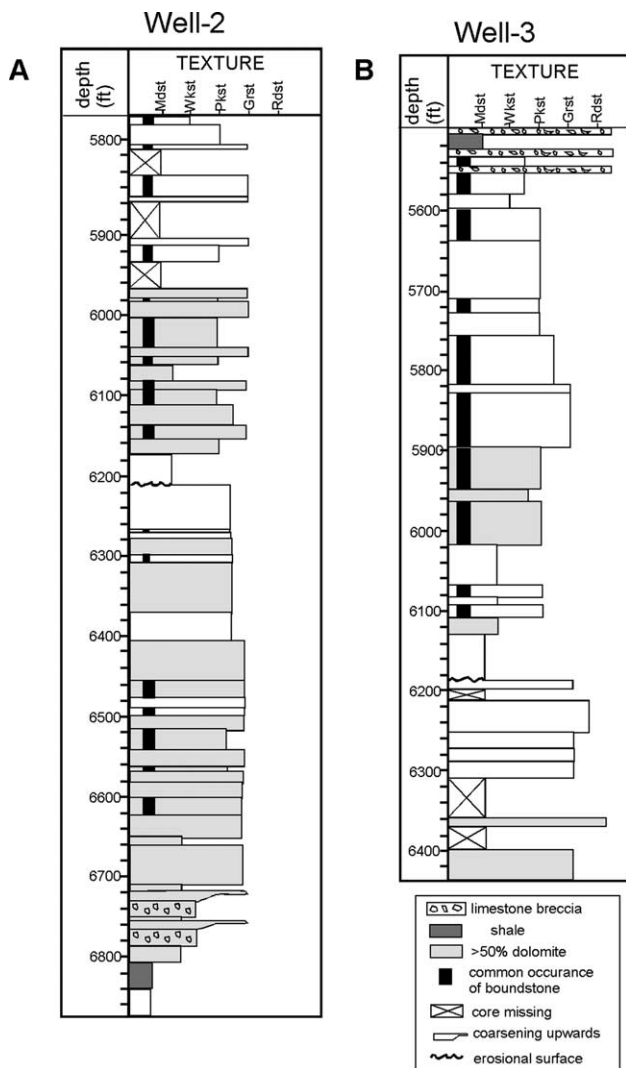
Fig. 5. Sedimentary logs of wells 2 and 3, subdivided by lithology and texture. Modified after Bracco Gartner (2000).
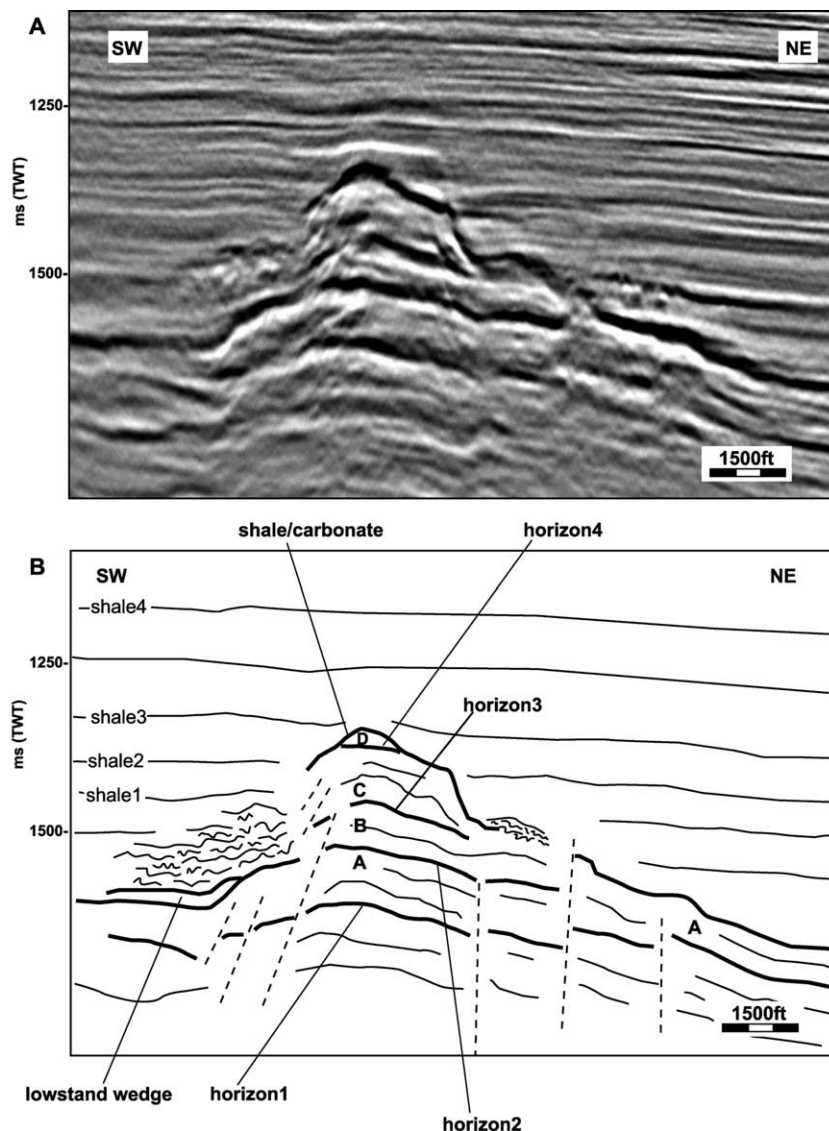
Fig. 6. (A) Uninterpreted seismic section through the studied Miocene platform. (B) Line drawing showing seismic horizon 1–4 and the seismic stratigraphic units labeled A–D. Dashed lines-faults. Wiggly reflectors-slide masses. Line location shown in Fig. 3.

Table 1
Seismic unit description

| Seismic unit	Bottom surface	Top surface	Seismic description	Sedimentologic interpretation
Unit A	Horizon 1	Horizon 2	$T = 70$ ms (TWT) low amplitude, discontinuous, mound-shaped on top of horizon 1	Horizon 1 = flooding event, horizon 2 = flooding event with associated backstepping and lowstand wedge. First phase of progradation (isolated patches prograded and coalesced in a larger flat-topped platform)
Unit B	Horizon 2	Horizon 3	$T = 68$ ms (TWT) low amplitude parallel continuous reflections interrupted by faults	Aggradation horizon 3 = flooding
Unit C	Horizon 3	Horizon 4	$T = 85$ ms (TWT) low amplitude, hummocky internal reflections, bodies of chaotic reflections associated with steep slopes	Aggradation coupled with progradation, slopes repeatedly collapsed in large landslides
Unit D	Horizon 4	Shale/carbonate	$T = 30$ ms (TWT) Convex upwards cap Horizon shale/carbonate = high amplitude. Internal reflections not resolved	Drowning
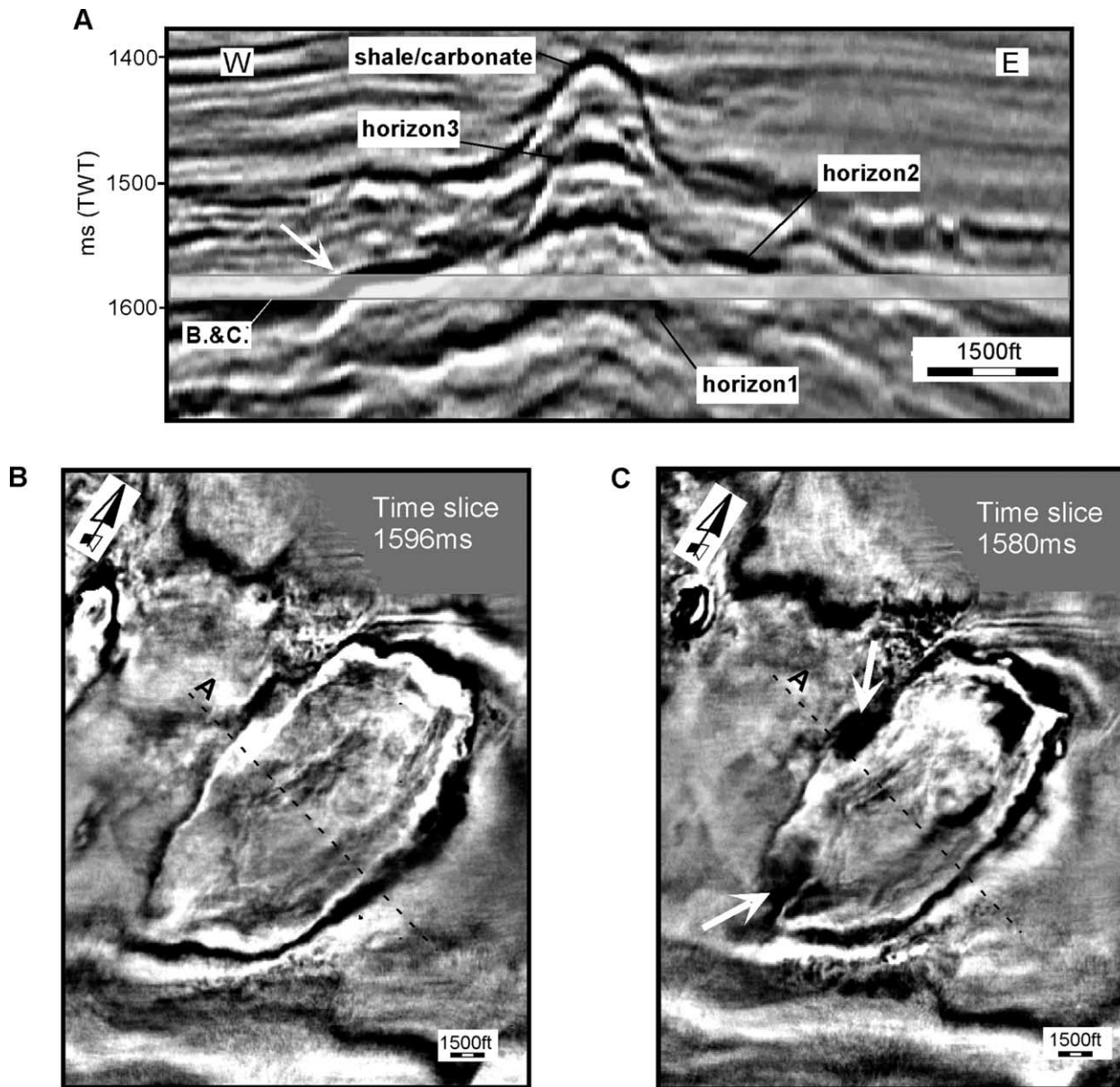
Fig. 7. The step (white arrow) on the vertical section (A) is interpreted to be a backstepping of the platform margin. Time-slices better show the evolution of the western margin from a straight (fracture controlled) trend (B) to the development of two concave structures as an initial phase of backstepping (C). Line location of A shown in both B and C.

Seismic *unit C*, between horizons 3 and 4, is characterized by low-amplitude hummocky reflections that are cut or deformed by faulting. The western margin is bounded by a sharp and steep slope. Basinwards of this steep slope there is a lens-shaped body of discontinuous, wavy reflections. This body wedges out both in downslope and upslope directions and is interpreted as a series of slumps. Several bodies of chaotic reflections can be identified on the flat basin floor. The youngest bodies wedge out near reflector shale 1. Horizon shale 2 smoothly covers the slides and onlaps the highest part of the platform. The eastern slope is steep but flattens in the lower part at the level of horizon 3 (Fig. 6),

where it is possible to map a smaller body characterized by chaotic reflections and wedge geometry.

Unit D lies between horizon 4 and the shale/carbonate reflectors. It has a thickness of 30 ms (TWT) and is too thin to show clear internal reflections. This unit represents the final stage of platform growth. At the top a high amplitude reflector (shale/carbonate marker) is shaped as a characteristic convex upward cap.

The correlation between the inner platform stratigraphy and the surrounding shale basin stratigraphy is not straightforward. Critical areas for the correlation are the flanks of the platforms with their faults and slide masses.
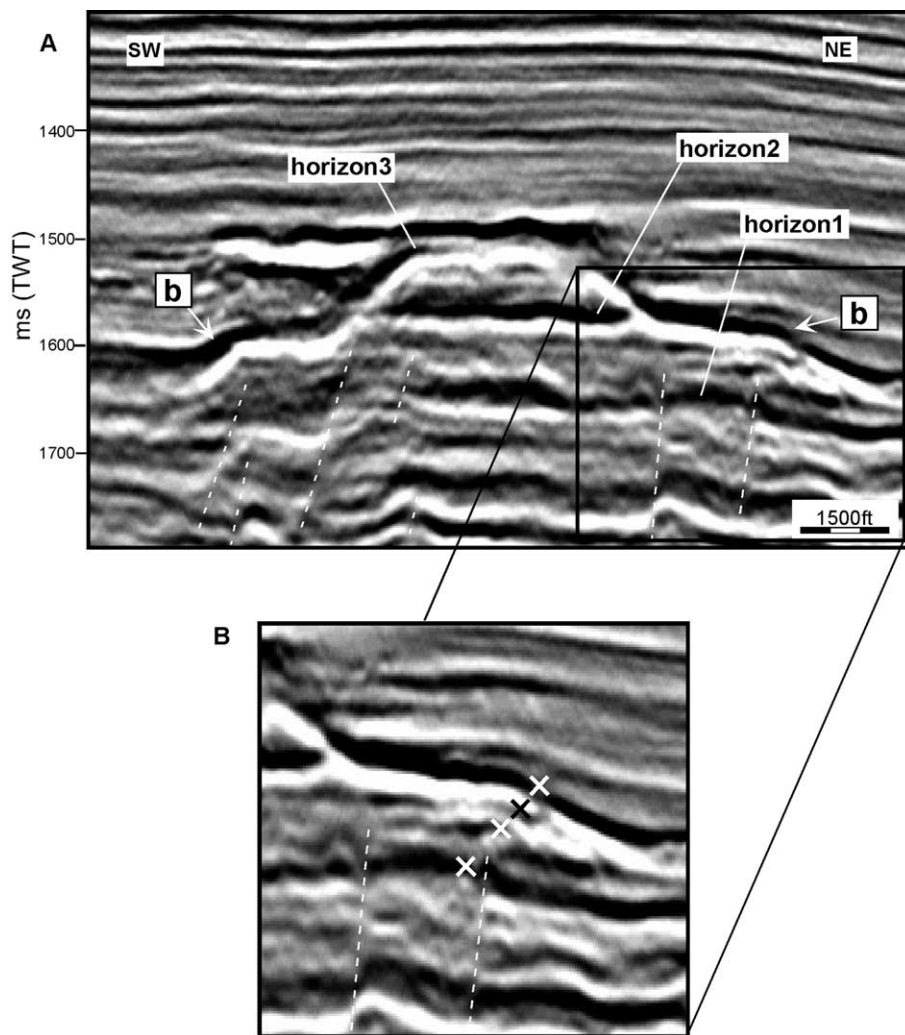
Fig. 8. (A) Vertical section showing backstepping at the platform margins (b) at horizon 2. At horizon 3 the platform backsteps again but the margin is out-of-section. That event appears as a flat flooding surface in this figure. (B) Inset showing the progradation on the eastern flank. Crosses mark the positions of the margin. The western flank is dissected by faults and margin positions cannot be identified. Line location shown in Fig. 3.

At the bottom of the platform edifice reflectors horizons 1 and 2 can be traced almost continuously from the platform domain into the shale domain (unit A). At the level of unit B there is no evidence of any significant slope lateral accretion. This suggests that horizon 3 merges with horizon 2. During times of slope progradation (unit C) repeated slumping destroyed the regular stratigraphic succession. The eastern and the western flanks are still affected by synsedimentary faulting. As a consequence, the stratigraphy established in the shale basin can only be approximately correlated with the platform (Fig. 6). Reflector shale 3 is the first marker that extends smoothly across the platform (Fig. 6).

5. Ties to wells

To tie the wells to the seismics, synthetic seismograms were generated for wells 2 and 3 (Fig. 4). Unfortunately wells 2 and 3 are located on the flanks of the carbonate platform and do not penetrate units C and D. We examined data from wells 2 and 3 with regards two prominent reflectors of the platform: shale/carbonate (Fig. 9) and horizon 2 (Fig. 10). In well 2, the shale/carbonate reflector coincides in the gamma-ray log with the boundary between slightly argillaceous carbonate below and marl and shale above. The same transition appears as an upward decrease in sonic velocity from approximately 4.5 to 2.5 km/s and in density from 2.7 to 2.1 g/cm^3. Synthetics show this boundary as a sharp, high-amplitude positive reflection. The situation in well 3 is similar but complicated by the fact that the main carbonate body is overlain by beds of marly sediments with thick intercalations of carbonate breccias (Fig. 5; Bracco Gartner, 2000).

The situation at reflector horizon 2 (Fig. 10) is significantly different. Log excursions are similar in magnitude but the changes in natural gamma radiation on the one hand and sonic/density/porosity on the other are not in step. Examination of thin sections from the interval confirms this mismatch. Thin sections indicate limestones
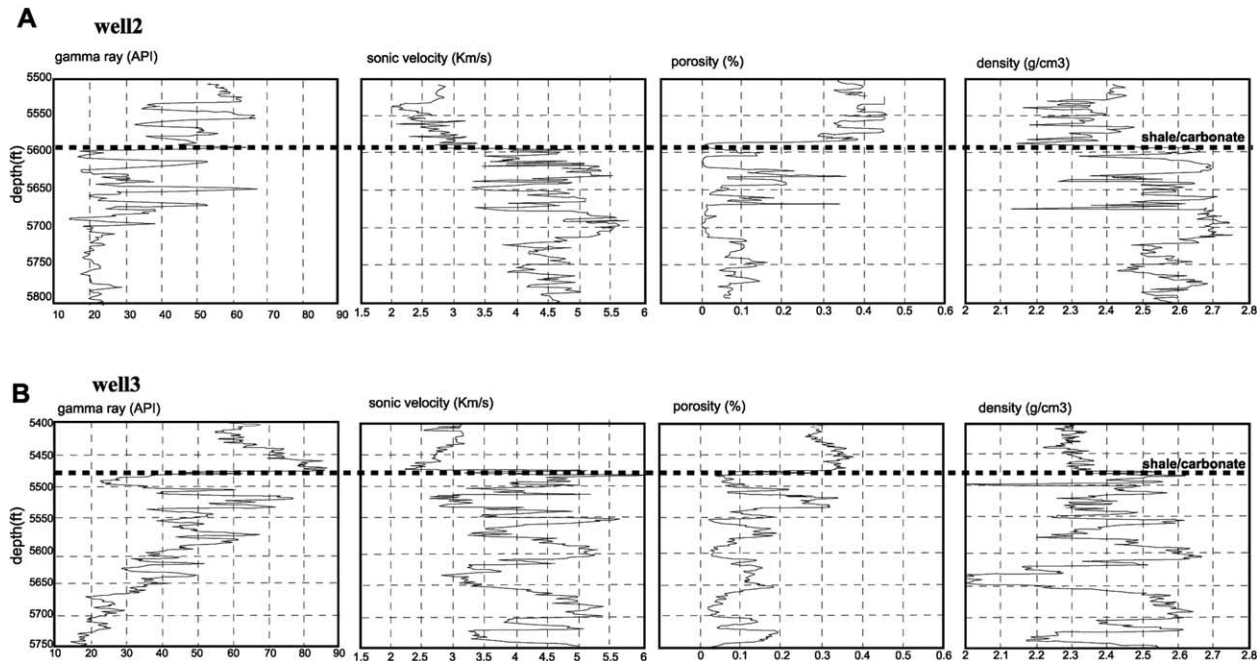
Fig. 9. Gamma ray, sonic velocity, neutron porosity and density logs from wells 2 (A) and 3 (B) were displayed in binary plots for depth intervals included the interpreted reflectors 'shale/carbonate'. The origin of the positive reflection for 'shale/carbonate' (black dashed line) is found in an impedance contrast at approximately 5590 ft for well 2 (A) and at 5477 ft for well 3 (B). A clear boundary between slightly argillaceous carbonate below and marl and shale above can be identified from the gamma ray, sonic velocity and density logs. The gamma-ray response drops below 50 Api units, density and sonic velocity increase at top of the carbonate interval (5590 ft in well 2 and 5577 ft in well 3).

with abundant clay laminae where the gamma-ray log shows a 100 ft (30 m) bundle of layers with moderately elevated readings. At about this depth, the logs also show an interval of elevated sonic velocity and density. However, the boundaries of this high-velocity, high-density interval do not correspond to the boundaries of the argillaceous limestones. Rather, the high-velocity/high-density interval extends upward beyond the upper boundary of the clay-rich limestones. The upper 60 ft (18 m) of the high-velocity/high-density unit show low gamma radiation while the lower part consists of the limestones with clay seams. Thin-section coverage is limited but it strongly suggests that the common denominator of the high-velocity zone is abundant late-diagenetic calcite cement. This cement makes up 30–50% of the thin-sectioned samples and creates a tightly interlocking mosaic of calcite crystals with less than 2% visible porosity in thin-sections. The offset between the boundaries of the clay-rich and the high-velocity intervals is best displayed in well 2 (Fig. 10A). In well 3 the situation is comparable but the gamma-ray log is poorly corrected because the hole diameter changes at about this level (Figs. 10B and 11).

6. Interpretation

6.1. Sedimentological interpretation

Horizons 2 and 3 consistently show a typical back-stepping geometry at the platform margins (Figs. 7 and 8A).

Backstepping indicates partial drowning and deep flooding of the platform, a process that often leads to increased deposition of terrigenous fines on the platform. Thus, the interpreted horizons in the platform correspond to flooding events (transgressive systems tracts) when slightly argillaceous, deeper-water material is deposited on top of clean carbonates, rich in well-winnowed patch reefs and lime sands. The development of such geometries is controlled by the interplay of two factors: the rate of carbonate production and growth and the rate of creation of new accommodation space. When the rate of creation of the accommodation space exceeds the growth potential of the platform, the platform backsteps trying to 'keep up' with the relative sea-level rise. Well logs and synthetic seismograms also indicate significant diagenetic overprinting of the flooding events (Figs. 4, 10 and 11). At least in some instances thin-sections reveal that the boundaries between low and high impedance intervals correspond to rapid transitions from highly porous to tightly cemented argillaceous limestone. This diagenetic overprint locally masks the depositional flooding event that deposited argillaceous limestone with deep-water biota on top of rather clean, shallow-water carbonates. Petrographic studies (Zampetti, Schlager, van Konijnenburg, and Everts, in press) indicate that (a) much of the porosity was created by dissolution under burial conditions, postdating a phase of extensive stylolitization; (b) the cement in the tight layers also postdates stylolitization and probably formed under elevated temperatures as the cementing minerals include saddle dolomite and fluorite
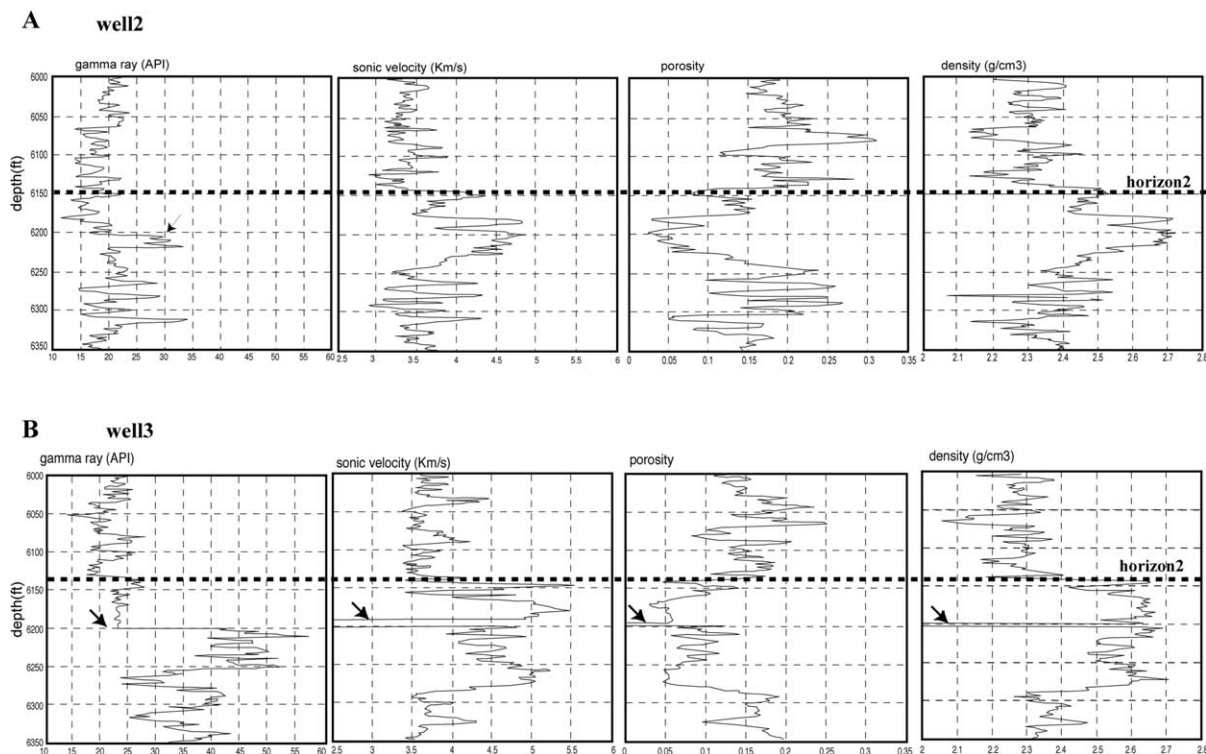
Fig. 10. Gamma ray, sonic velocity, neutron porosity and density logs from wells 2 (A) and 3 (B) were displayed in binary plots for depth intervals included the interpreted reflectors 'horizon 2' (black dashed line). Significant changes in natural gamma-ray radiation and sonic/density/porosity are not in step. Well 2 (A) shows elevated sonic velocity and density values below 6140 ft. The gamma ray shows a significant change at 6200 ft (black arrow), 50 ft below the change in velocity and density. The gamma-ray log in well 3 (B) shows a dramatic increase in value from 6200 ft, downwards. Taking into account the data gap in this interval for the sonic, the density and the porosity (arrows) related to a change in borehole diameter as observed in the caliper log from this depth onwards, the absolute values of the gamma-ray log below 6200 ft may be not reliable. Thin sections indicate that the boundary between low and high impedance interval correspond to rapid transition from highly porous to tightly cemented argillaceous limestone. Thus the seismic reflection at the well location seems to coincide with a diagenetic boundary.

(see Section 7). The diagenetic boundary may differ by 15 m in elevation from the facies boundary between clean carbonate and slightly argillaceous carbonates (Fig. 10). However, with the available data it is not possible to determine how laterally continuous the diagenetic pattern is and how far its boundaries deviate from the depositional layering.

In addition to flooding, subaerial exposure events also influenced the platform architecture, but their seismic expression is less prominent. There is fairly good geometric evidence of a lowstand systems tract (Fig. 6) indicating relative sea-level fall prior to rapid flooding and back-stepping at horizon 2. We have no seismic evidence that flooding at horizons 3 and 4 were also preceded by exposure (Fig. 6), but we cannot exclude this possibility either.

Seismic unit C is characterized by aggradation coupled with progradation of the platform flanks. The prograding clinoforms were repeatedly affected by large-scale sliding and slumping. Slide masses can be traced seismically for about 1.5 km (5000 ft) into the basin. They appear as lobe-shaped bodies of chaotic and wavy reflections (Hine et al., 1992, 1994; van Weering, Nielsen, Kenyon, Akentieva, & Kuijpers, 1998). The landslides appear to be triggered by faults. Hine et al. (1994), Nicaragua Rise, and Drzewiecki
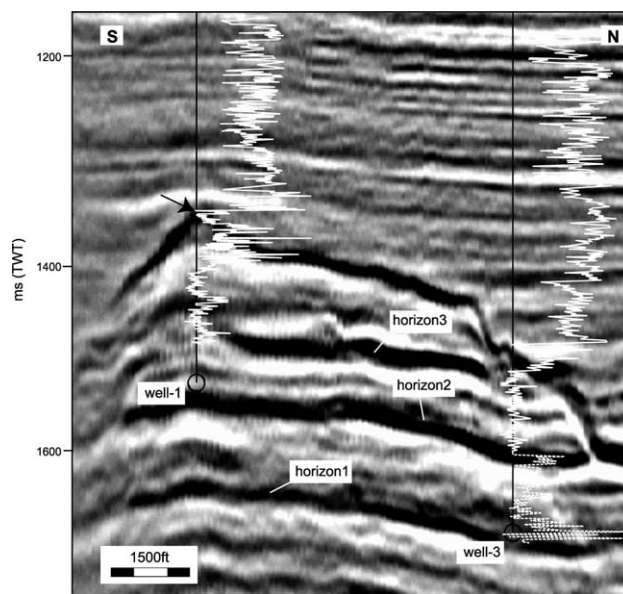

Fig. 11. Gamma ray logs for two of the three vertical wells tied to a N–S trending seismic section. Note that for well 1 the shift (black arrow) in gamma ray is exactly on top of the shale/carbonate reflector interpreted as drowning surface. The gamma-ray log in well 3 shows a significant increase in value downward at 'horizon 2' (broken line). However, the log scale below horizon 2 is doubtful because of a bit change at this level. The absolute values of the gamma ray, therefore, may not be reliable. Line location shown in Fig. 3.

and Simò (2002), Pyrenees, relate similar events to well-documented tectonic activity.

Unit D represents the final stage of the platform growth. It is characterized by smooth and convex upwards reflections suggesting that the platform was drowned by gradually subsiding below the zone of wave action.

Fig. 12 summarizes the growth history of the platform in the form of a generalized NE–SW section. The dominant pattern is flat-topped upward growth, coupled with back-stepping of the margins. During the growth cycle of the platform, the platform-basin relief increased from about 45 ms (about 50 m or 164 ft) at level of horizon 2 to 220 ms (about 450 m or 1475 ft) above the basin floor at the time of horizon 4. Two phases of progradation were inferred based on the combined interpretation of the seismic and well information. The first progradation occurred in unit A where isolated carbonate patches (Figs. 8B and 13) first rose above the surrounding sea floor, then prograded and coalesced to form one large flat-topped platform that prograded further to the margin positions visible on reflector horizon 2.

The second phase of progradation is unit C. At that time slopes were high and steep and repeatedly collapsed into large submarine landslides possibly triggered by faulting. During the final stages of growth (post-horizon 4; Fig. 12), the platform changed from flat-topped to mound-shaped. In this particular case, we interpreted the change from platform to mound by submergence below the zone of intensive wave action and finally below the photic zone (Fig. 14).

6.2. Faulting

Faulting affected the entire area covered by the 3D survey, but the deformation seems to be more pervasive at the eastern and western boundaries of the studied platform. The dominant fault system strikes from 015°–040° to 040°–070° and a subordinate system strikes 350°–360° (Fig. 15). The majority of the faults are low-offset, closely spaced, steep W- or NW-dipping normal faults. Seismics clearly show faulting to be partly coeval with platform growth and to hardly affect the overlying shale (Fig. 15A). Faulting
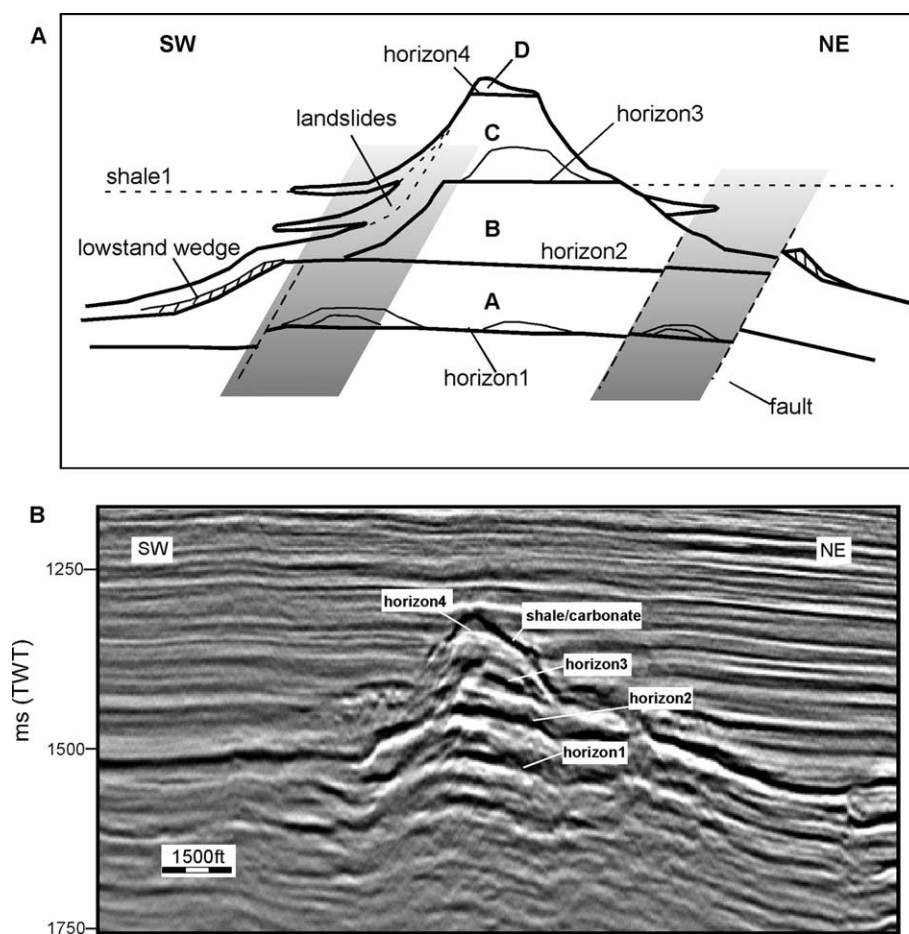

Fig. 12. Model of the platform growth history proposed in this study (A) compared with a seismic section (B). The dominant pattern consists of flat-topped upward growth. In the time seismic sections horizons 1, 2 and 3 are not flat due to velocity pull-up effects. Two main phases of progradation were identified: the first one occurred at level of horizon 1 when isolated carbonate patches prograded and coalesced to one large platform. During the second phase of progradation slopes were high and steep and collapsed into large landslides (dashed lines and stringers) guided by faults (grey bands). The growth history is characterized by alternation of flooding, associated with backstepping (horizon 2) and exposure events, associated with lowstand tracts (striped bands). In the final stages of the growth the platform changed from a flat-topped to a mound-shaped, indicating submergence and drowning.
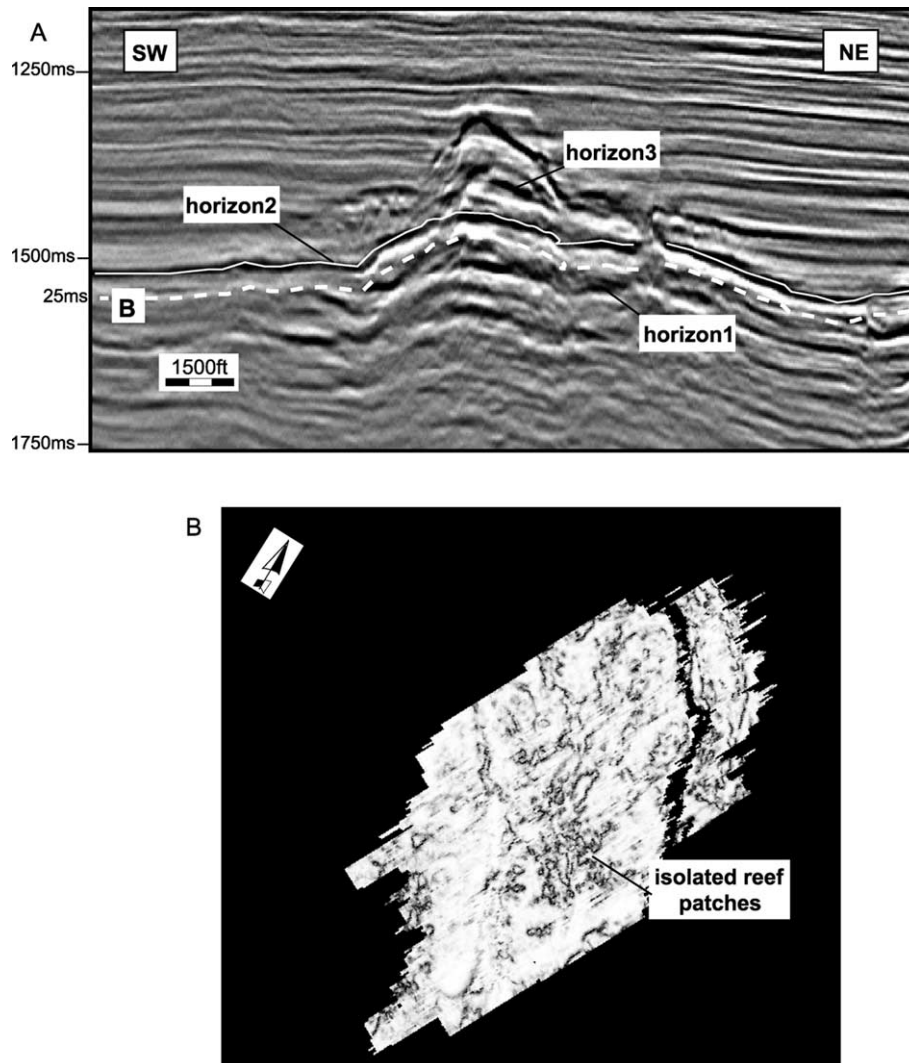
Fig. 13. The first phase of progradation occurred between horizon 1 and horizon 2 when isolated reef patches rose above the surrounding sea floor and then prograded and coalesced in a larger platform and it is clearly shown in a horizon slice display (B). The location of the horizon slice cutting 25 ms below horizon 2 is shown in cross section (A, white dashed line). Line location shown in Fig. 3.

seems also to govern the north-south elongation of the platform. The narrow northern and southern flanks occupy the space between two fault zones. The very top of the studied platform (unit D) is hardly affected by faulting and appears as a smooth and convex upward surface (Fig. 14).

6.3. Slope geometry

Time-depth conversion was performed on selected sections to constrain our interpretation and to estimate slope angles and fault dips (Fig. 16). In depth sections, the inner platform reflections horizons 1, 2, 3 and 4 are flat and nearly horizontal. The bending in time sections is thus related to a velocity pull-up and the platform had a flat top during all but the final stage of growth. In depth-converted sections, the contrast between a flat-topped platform and the distinctly convex geometry of the final stages of growth becomes more obvious than in time sections. Horizon 4 is the last nearly

horizontal reflection in the platform and it is interpreted as the last backstep followed by gradual drowning. The western flank is still characterized by a lowstand systems tract seaward of the backstep at the level of horizon 2, and by chaotic reflections interpreted to be slide masses. The exceptionally steep, strongly concave segment on the eastern flank is interpreted as slide scar. After time-to-depth conversion, faults are still clearly visible and can be mapped. The dip direction is the same as in the time sections but with reduced offset and inclination (Fig. 16).

Estimate of slope angles was carried out on depth-converted sections where velocity effects were eliminated or at least minimized. The use of 2D sections, however, still introduces some uncertainty on the true slope angles. Slope inclination varied through time during the different growth stages. Fig. 16 and Table 2 document slope angles for different segments of the platform flanks. After time-depth conversion, the slope at about 5750 ft depth (1.56 ms) on
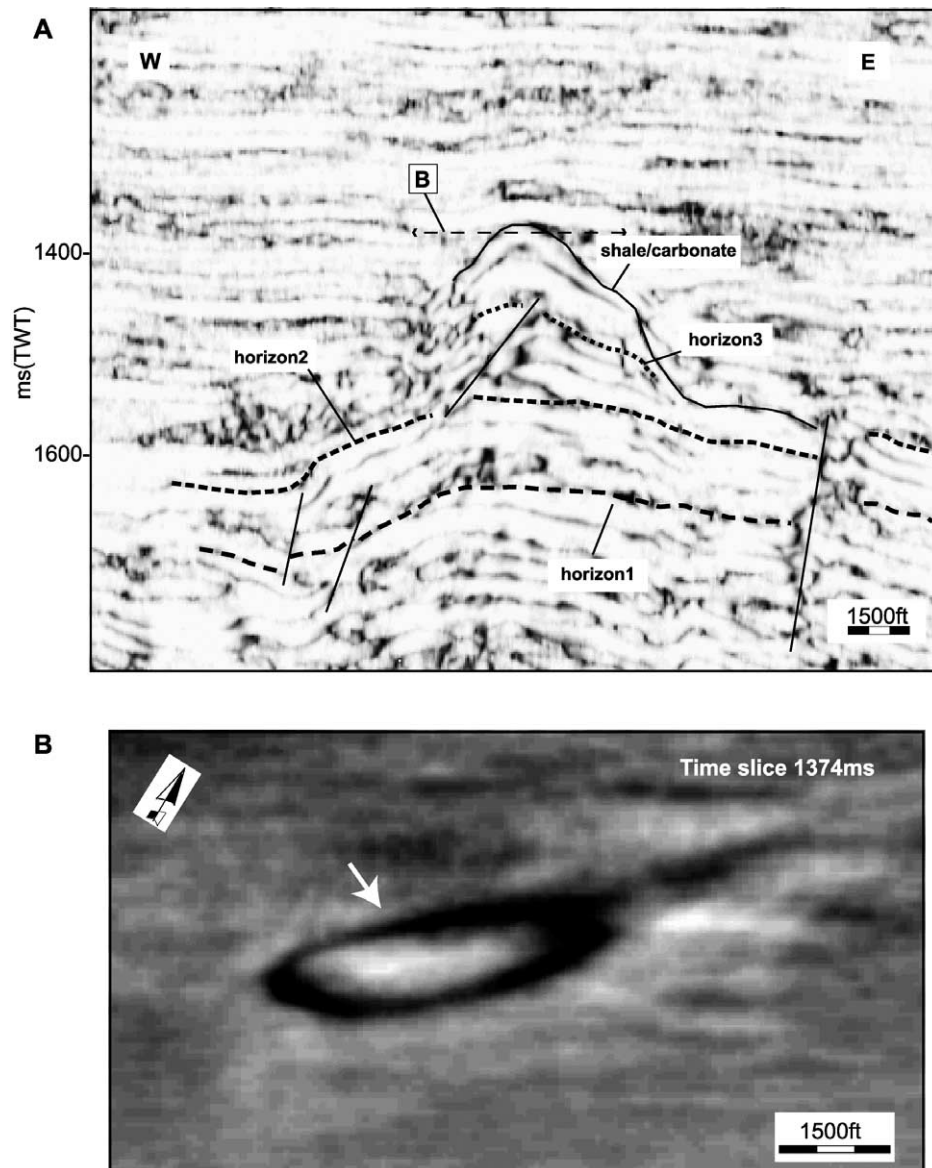
Fig. 14. In the final stages of the growth the platform changed to a mound-shaped top (A, black arrow) indicating submergence below the zone of intensive wave action and finally below the photic zone. Variance attribute cross-section (A) and reflection time slice (B) perfectly show this characteristic geometry. Location of time slice (B) shown as dashed line in (A). Line location shown in Fig. 3.

the northern flank shows an inclination of 12° in contrast with the previous interpretation of 25° by Bracco Gartner (2000). The southern side has a uniform angle of 14° and the particular geometry of the slope suggests that it was exposed to wind and wave actions (Bracco Gartner, 2000).

Kenter (1990) described the relationship between slope angles and sediment fabric. His data show that the slope angle of carbonate platform flanks is strongly related to the sediment fabric making up the slope volume. Grain-supported fabrics support steeper slopes than muddy cohesive fabrics. Maximum slope angles, varying between 30° and 40°, are found within the grainy mud-free cohesionless fabrics. Slope angles in the muddy fabric category drop to values below 15° for mud-supported fabric and under 5° for pure mud (Kenter, 1990).

Data from literature (Kenter, 1990) suggest that measured angles ranging from 12° to 19° (Table 2) are related to a grain-supported sediment fabric with mud matrix. Slopes with angles below 4° plot within the muddy fabric category.

Our seismic data indicate that extrinsic factors rather than sediment fabric control the steeper slope angles in the studied platform. The steep slope on the western flank (35°) corresponds to a fault plane (Fig. 16A and Table 2). The dip of the slope is therefore the inclination of the fault. On the eastern and on the northern sides (Fig. 16 and Table 2) the steep segments of the flanks are interpreted as slide scars. The slide scars cut deeper in the substrate affecting more compacted material. This allows the platform to maintain a steeper slope even if the original sediment was mud
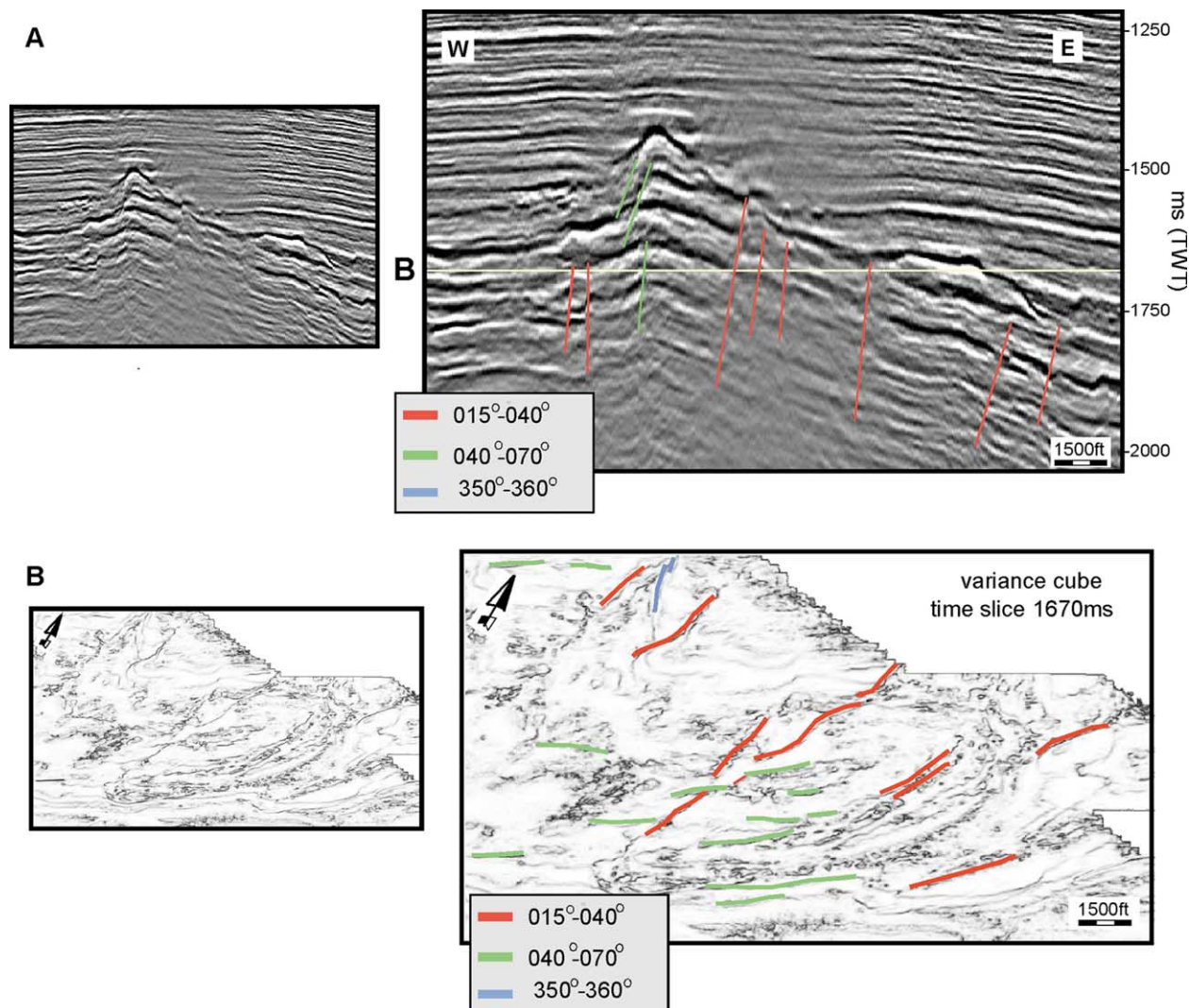
Fig. 15. (A) Seismic line showing fault sets. The different systems are labelled by fault strikes. The majority of the faults are steep, low-offset W or N–W-dipping normal faults. (B) Time slice from variance cube showing plan view of the fault systems. Deformation affects the entire area but it seems to be more pervasive around and in the platform. Line location shown in Fig. 3.

and, therefore, the slope angle does not directly depend on the sediment fabric.

7. Discussion

The high quality of the 3D seismic data used in this study and the consequent possibility of applying techniques such as variance cube, horizon slice and time-depth conversion largely explains the differences with earlier studies regarding the main processes affecting and controlling the growth of this Miocene carbonate platform. Below, we discuss the most important differences.

7.1. Faulting

The understanding of the effect of faulting on platform growth has improved with respect to the older 2D data used

by Bracco Gartner (2000), Epting (1989) and Vahrenkamp (1996, 1998). These authors assumed that the development of the platform was essentially unaffected by tectonic deformation and that Luconia platform growth was governed by eustatic sea-level fluctuation.

Our interpretation suggests that platform distribution was largely governed by faults and tilted blocks, and that the growth architecture of the platform, too, was affected by syndepositional faulting. Other examples of Tertiary fault-block carbonate platforms in SE Asia, such as Qamar Basin (Yemen; Brannan, Gerdes, & Newth, 1997), Kutei Basin (Indonesia; van der Weerd & Armin, 1992) and Tonasa Platform (Indonesia; Wilson, Bosence, & Limborg, 2000) indicate that these platforms were not only located on basement highs related to earlier structures, but also that they were affected by syndepositional faulting that influenced their vertical and lateral accretion and the geometry of the platform margins. Particularly in the studied platform
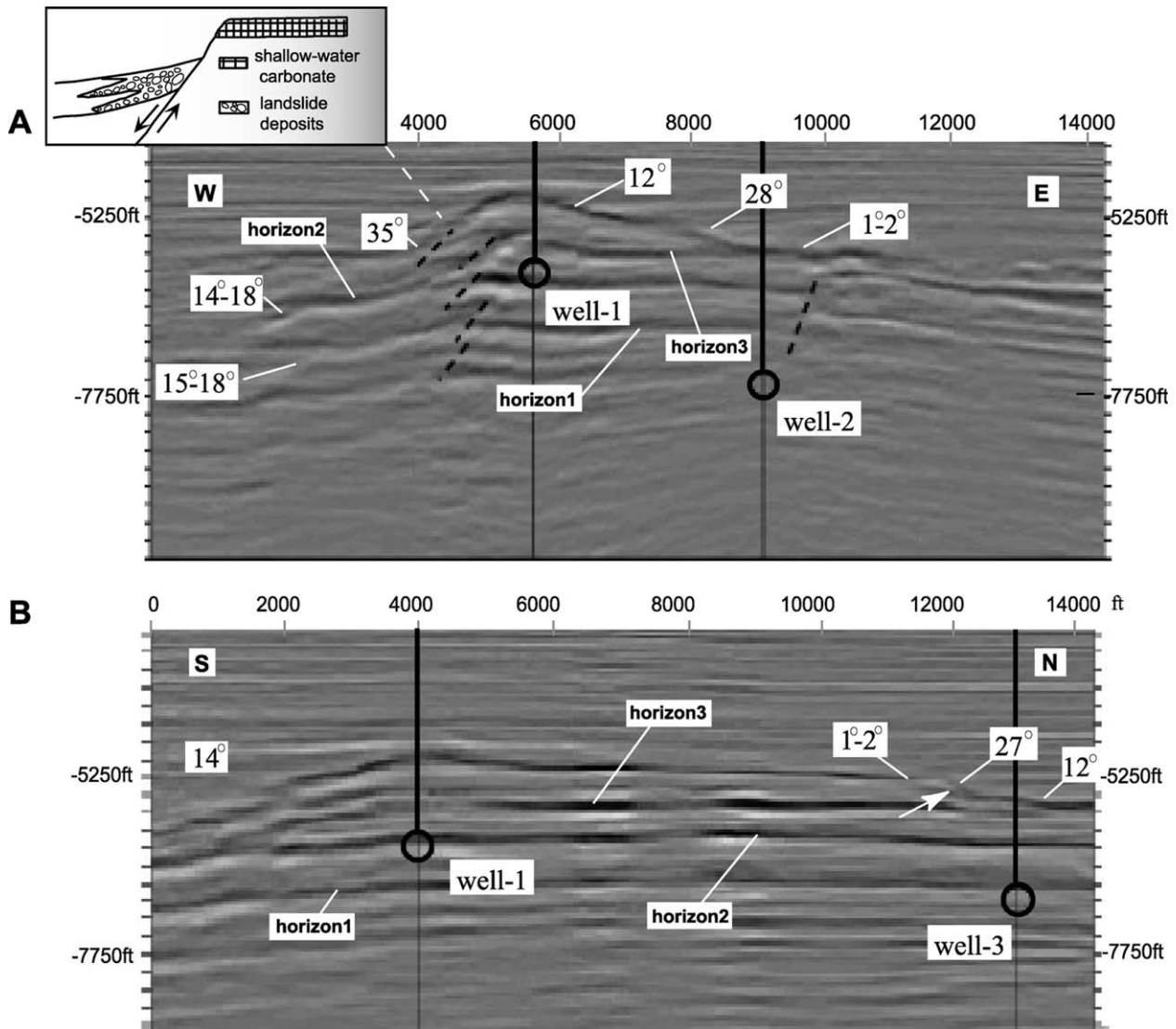
Fig. 16. Slope angles in depth-converted sections. (A) E–W section. On the western side of the platform slope angles are 15°–18° at level of horizon 1, 14°–18° at level of horizon 2, and 35° at level of unit B. The eastern flank starts at the top with a slope of 12°, increases to 28° at level of unit C, decreases in a gentle slope dipping 1°–2°. B. N–S section. The northern flank is characterized by a gentle slope (1°–2°) at the top, increases to a maximum 27° at level of unit C, and decreases to 12° at level of unit (B) After time-depth conversion, the slope at 1.56 ms on the northern flank shows an inclination of 12° (arrow) in contrast with the previous interpretation of a 25° inclined, small bypasses or erosional slope (Bracco Gartner, 2000). The southern side has a uniform angle of 14° and its particular geometry clearly suggests that it was exposed to wind and wave actions (Bracco Gartner, 2000). Line location shown in Fig. 3.

the broad western and eastern flanks were controlled by low-offset faults that were active during platform growth (Fig. 15). The narrow northern and southern flanks occupy the space between two fault zones (Fig. 15). The fault zones indeed seem to govern the pronounced N–S elongation of the platform (Fig. 17). In addition, N or NW directed currents may have accentuated the pattern (see below).

7.2. Tilting

Several seismic sections give the impression that the platform top is somewhat tilted and onlapped by shale reflections (Fig. 6). However, we cannot substantiate such a tilt as depth-migrated sections show the platform top to be

Table 2
Estimates of slope angles from depth-converted vertical sections (Fig. 16)

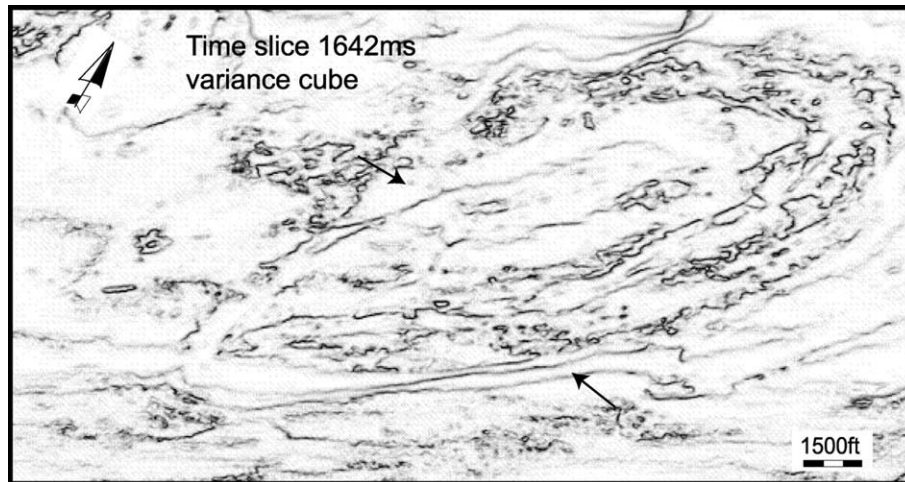| Location	Nr.	Slope angles (°)	Max slope angles	Interpretation
Southern flank		14	17°	Depositional
Northern flank	1	1–2		Depositional
	2	27		Slide scar
	3	12		Depositional
Eastern flank	1	12		Depositional
	2	28		Slide scar
	3	1–2		Depositional
Western flank	1	14	35°	Fault plane
	2	15	18°	Depositional
	3		18°	Depositional

Fig. 17. Time slice from variance cube. The fault zones (black arrows) seem to govern the typical N–S elongation of the platform, further modulated by currents.

essentially flat and parallel to the shale reflections. The impression of tilt and onlap is, in our opinion, created by three effects: (1) Velocity pull-up by the overlying carbonate rocks; (2) sediment accumulations at the toe of the newly established slope after a backstep; (3) scours forming near the margins of the platform by local eddies and are subsequently filled by very gently dipping clinoforms of shale.

7.3. Flank erosion

Bracco Gartner (2000) suggested that during platform growth the southern flank may have been erosional and was onlapped and buried by shale after platform drowning. He attributed the erosion to scouring by turbidity currents that were transporting excess sediment from the platform to the basin. Based on 3D mapping, we believe that the southern flank is too narrow and too convex to capture many turbidity currents. It may have been eroded by contour currents instead. The higher elevation of the southern part of the platform and the higher declivity of its southern slope also suggest that the southern platform margin faced up-current as already suggested by Bracco Gartner (2000) and also described by Erlich, Barrett, and Ju (1990) for the Miocene Liuhua platform in the Pearl River Mouth basin. Self-erosion of the platform flanks does occur in the studied platform but mainly on the west- and east-facing slopes, where it is driven by slope failure and slumping during periods of progradation and syndepositional faulting. Purdy and Bertram (1993) indicated such a model for the truncation of platform slopes in the Maldives. In addition, outcrop studies in Gulf of Suez (Bosence, Cross, & Hardy, 1998; Burchette, 1988) and Indonesia (Wilson et al., 2000) indicate that boundary syndepositional faulting movements lead to shedding of coarse, immature and redeposited material.

7.4. Drowning and subaerial exposure

Drowning of the Luconia carbonate platforms has been attributed to decreasing water quality and increasing subsidence (Fulthorpe & Schlanger, 1989) in front of the advancing siliciclastic wedges with pronounced backstepping of the platform during final growth phases (build-in phase of Epting, 1980). Vahrenkamp (1996, 1998) assumed that the final cessation of carbonate growth is coeval throughout the Central Luconia Province and that the carbonate platforms were terminated by subaerial exposure reflecting the eustatic sea-level fall at the end of the Middle Miocene (Haq, Hardenbol, & Vail, 1987). For the studied platform we see two problems with the exposure interpretation. First, in the youngest parts of the platform we found no seismic evidence of exposure in the form of lowstand systems tracts, erosional terraces or dolinas (Moldovanyi, Wall, & Zhang, 1995; Story, Peng, Heubeck, Sullivan, & Dong Lin, 2000). On the contrary, the uppermost part of the platform shows very smooth reflections (particularly well displayed in time slices) that change upward from horizontal to convex. We interpret this as a change from a flat-topped platform that grew in the zone of intensive wave action to a mound that gradually subsided below wave base. Second, the platform is covered by deeper-water shale. Thus, even if exposure interrupted growth, the carbonate system must have been drowned when marine conditions were re-established.

We conclude that there is no seismic and log evidence to support a subaerial exposure event associated with the drowning of the platform. Smooth, concentric reflectors forming a convex mound onlapped by sub-horizontal basinal shale reflectors strongly suggest gradual drowning possibly followed by a deeper-water hardground. Geologically the drowning unconformity has been described as an abrupt shift from shallow-water carbonate deposition to siliciclastic deposition (Erlich et al., 1990; Schlager, 1989).

Ties between seismics and well logs for the study platform suggest that the high amplitude reflector interpreted as drowning unconformity corresponds to a lithological change between carbonates and siliciclastics (Fig. 11). Similar situations have been described for the Miocene Porong platform (Madura Strait, Indonesia; Kusumastuti, van Rensbergen, & Warren, 2002) and for the Miocene Liuhua platform (South China Sea; Erlich et al., 1990).

The drowning of the studied platform may have been caused by a rapid relative rise in sea level (Fulthorpe & Schlanger, 1989) or by reduction of carbonate production due to the increased nutrient levels (Mutti & Hallock, 2003).

Epting (1989) and Vahrenkamp (1996; 1998) also described pronounced exposure events from deeper stratigraphic levels of the platform, older than the final drowning succession. We agree with these authors that from what is known about Miocene eustacy, repeated exposure of the platform is very likely and for horizon 2 we can also provide seismic evidence in the form of occasional lowstand systems tracts. At the other horizons, however, we did not find seismic evidence of exposure. Moreover, two of Epting's and Vahrenkamp's arguments for exposure-limestone breccias on the flanks and horizons with extensive secondary porosity and blocky calcite cement on the platform-should no longer be considered diagnostic criteria for exposure in the case of the studied platform. We have shown above that the breccias are the result of slope failure during a phase of rapid platform progradation and that synsedimentary faulting is a likely trigger. Petrographic studies show that the vast majority of secondary porosity and calcite cements in the platform deposits were created by dissolution/precipitation from warm fluids during deep burial rather than exposure (Zampetti, Schlager, van Konijnenburg, & Everts, in press). Late-leaching porosity is closely associated with stylolites and concomitant fractures. This dissolution event is generally not grain selective, probably because it affected a rock where aragonite and most magnesian calcite had already stabilized to calcite or had been converted to dolomite. The leaching clearly postdates much of the pressure solution. It produces vugs and solution channels that represent modified compaction fractures (Zampetti, et al., in press). A model for extensive leaching of carbonates under burial, termed mixing corrosion, has been advocated for the Tertiary limestones of The Bombay High (Esteban & Taberner, 2003; Minero, Esteban, Sarmiento, & Kumar, 2000). According to this model, porosity is created when resident pore fluids mix with warmer hydrothermal fluids rising from depth.

8. Conclusions

Detailed seismic analysis of a high-resolution 3D data set and wireline logs from three vertical wells of a Luconia carbonate platform have shown a well-defined build-up characterized by a dominant pattern consisting of upward growth with a flat top, coupled with backstepping of the margins and two main phases of progradation.

During the first phase (unit A), isolated carbonate patches rose, prograded and merged to form one flat-topped large platform. Slope angles range from 14° to 15° suggesting a muddy grain-supported fabric of the slope deposits. The second phase of progradation (unit C) is characterized by a high and steep slope (27°–35°) that repeatedly collapsed in large submarine landslide masses probably guided by syndepositional faulting. Such steep slope angles are probably related to extrinsic factors, because they coincide either with slide scars or fault planes. Faulting influenced platform distribution and growth architecture of the platform and its characteristic N–S elongation.

Main reflectors in the platform correspond to flooding events. Exposure prior to the flooding could be demonstrated for only one key horizon. At the other marker horizons, exposure events were either absent or too short to produce seismically recognizable patterns.

The change from a flat-topped to mound-shaped platform top indicates gradual submergence below the zone of wave action and final drowning of the platform. Smooth, concentric, high amplitude reflectors forming a convex cap onlapped by basinal shales suggest final drowning of the platform without interruptions by major exposure events.

Acknowledgements

References

Aigner, T., Doyle, M., Lawrence, D., Epting, M., & van Vliet, A. (1989). Quantitative modeling of carbonate platforms: some examples. In P. D. Crevello, J. L. Wilson, J. F. Sarg, & J. F. Read (Eds.), *Controls in carbonate platform and basin development* (pp. 27–37). *Society of Economic Paleontologists and Mineralogists, Special Publication No. 44*.

Brannam, J., Gerdes, K. D., & Newth, I. R. (1997). Tectno-stratigraphic development of Qamar Basin, Eastern Yemen. *Marine and Petroleum Geology, 14*, 701–730.

Bosence, D. W. J., Cross, N., & Hardy, S. (1998). Architecture and depositional sequences of Tertiary fault-block carbonate platforms; an

analysis from outcrop (Miocene, Gulf of Suez) and computer modelling). *Marine and Petroleum Geology*, 15, 203–221.

Bracco Gartner, G. L (2000). *High resolution impedance model of outcrops and their application in seismic interpretation.* PhD Thesis. Vrije Universiteit, Amsterdam. pp. 105–123.

Burchette, T. P. (1988). Tectonic control on carbonate platform facies distribution and sequence development: Miocene, Gulf of Suez. *Sedimentary Geology*, 59, 179–204.

Doust, H. (1981). Geology and exploration history of offshore central Sarawak. In M. T. Halbouty (Ed.), *Energy resources of the Pacific region* (pp. 117–132). *AAPG (Tulsa), Studies in Geology.*

Drzewiecki, P. A., & Simò, J. A. (2002). Depositional processes, triggering mechanisms and sediment composition of gravity flow deposits: examples from the Late Creatceous of south-central Pirenees, Spain. *Sedimentary Geology*, 146, 155–189.

Epting, M. (1980). Sedimentology of Miocene carbonate buildups, central Luconia, offshore Sarawak. *Buletin Persatuan Geologi Malaysia = Bulletin Geological Society of Malaysia*, 12, 17–30.

Epting, M. (1989). The Miocene carbonate buildups of central Luconia, offshore Sarawak. In A. W. Bally (Ed.), *Atlas of seismic stratigraphy* (pp. 168–173). *AAPG (Tulsa). Studies in Geology.*

Erlich, R. N., Barrett, S. F., & Ju, G. B. (1990). Seismic and geologic characteristics of drowning events on carbonate platforms. *AAPG Bulletin*, 74(10), 1523–1537.

Esteban, M., & Taberner, C. (2003). Secondary porosity development during late burial in carbonate reservoirs as a result of mixing and/or cooling of brines. *Journal of Geochemical Exploration*, 78–79, 355–359.

Fulthorpe, C. S., & Schlanger, S. O. (1989). Paleo-ocenagraphic and tectonic settings of early Miocene reefs and associated carbonates of offshore Southeast Asia. *AAPG Bulletin*, 73(6), 729–756.

Hall, R. (1996). *Reconstructing Cenozoic SE Asia. Geological Society of London Special Publications 106*, pp.153–184.

Haq, B. U., Hardenbol, J., & Vail, P. R. (1987). Chronology of fluctuating sea level since the Triassic. *Science*, 235, 1156–1167.

Hine, A. C., Harris, M. W., Locker, S. D., Hallock, P., Peebles, M., Tedesco, L., Mullins, H. T., Snyder, S. W., Belknap, D. F., Gonzales, J. L., Neumann, A. C., & Martinez, J. (1994). Sedimentary infilling of an open seaway: Bawihka Channel, Nicaraguan Rise. *Journal of Sedimentary Research*, 64(1), 2–25.

Hine, A. C., Locker, S. D., Tedesco, L. P. M., Mullins, H.P., Hallock, P., Belknap, D. F., Gonzales, J. L., Neumann, A. C., & Snyder, S. W. (1992). Megabreccia shedding from modern, low-relief carbonate platforms—Nicaraguan Rise. *Geological Society of America Bulletin*, 104, 928–943.

Hutchison, C. S. (1989). *Geological evolution of South East Asia. Monographs on Geology and Geophysics*, Oxford: Oxford University Press.

Kenter, J. A. M. (1990). Carbonate platform flanks: slope angle and sediment fabric. *Sedimentology*, 37, 777–794.

Kusumastuti, A., van Rensbergen, P., & Warren, J. K. (2002). Seismic sequence analysis and reservoir potential of drowned Miocene carbonate platforms in the Madura Strait, East Java, Indonesia. *AAPG Bulletin*, 86(2), 213–232.

Lee, T., & Lawver, L. A. (1995). Cenozoic plate reconstruction of South East Asia. South-East Asia structures and tectonics. *Tectonophysics*, 251, 1711–1735.

Minero, C. J., Esteban, M., Sarmiento, E. R., & Kumar, H. (2000). Burial porosity reservoirs in Bassein Formation, Bomabay Basin, offshore India. *AAPG Bulletin*, 84(9), 1465–1466.

Moldovanyi, E. P., Wall, M., & Zhang, J. Y. (1995). Regional exposure events and platform evolution of the Zhujiang Formation carbonates, Pearl River Mouth Basin: evidence from primary and diagenetic seismic facies. In D. A. Budd, A. H. Saller, & P. M. Harris (Eds.), *Unconformities and porosity in carbonate strata* (pp. 125–140). *American Association Petroleum Geologists, Tulsa, Memoir 63.*

Mutti, M., & Hallock, P. (2003). Carbonate systems along nutrient and temperature gradients: some sedimentological and geochemical constraints. *International Journal of Earth Sciences*, 92(4), 465–475.

Purdy, E. G., Bertram, G. T (1993). Carbonate concepts from the Maldives, Indian Ocean (pp. 57), *AAPG (Tulsa), Studies in Geology.*

Schlager, W. (1989). Drowning unconformities on carbonate platforms. In P. D. Crevello, J. L. Wilson, J. F. Sarg, & J. F. Read (Eds.), *Controls on carbonate platform and basin development* (pp. 15–25). *Society of Economic Paleontologists and Mineralogists, Special Publication No. 44.*

Sheriff, R. E. (1977). Limitations on resolution of seismic reflections and geological detail derivable from them. In C. E. Payton (Ed.), *Seismic stratigraphy—applications to hydrocarbon exploration* (pp. 3–14). *AAPG (Tulsa), Memoir 26.*

Story, C., Peng, P., Heubeck, C., Sullivan, C., & Dong Lin, J. (2000). Liuhua 11-1 Field, South China Sea: a shallow carbonate reservoir develop using ultrahigh-resolution 3D seismic, inversion, and attribute-based reservoir modelling. *The Leading Edge*, 19(8), 834–846.

Taylor, B., & Hayes, D. E. (1983). Origin and history of the South China Sea basin. In D. E. Hayes (Ed.), *The tectonic and geological evolution of southeast Asia seas and islands, part 2* (pp. 23–56). Washington: American Geophysical Union.

Vahrenkamp, V. C (1996). Miocene carbonates of Luconia Province, offshore Sarawak: implication for regional geology and reservoir properties from strontium isotope stratigraphy. *Petronas Research and Technology Forum.*

Vahrenkamp, V. C (1998). Sr-isotope stratigraphy of Miocene carbonates, Luconia Province, Sarawak, Malaysia; implications for platform growth and demise and regional reservoir behavior. In: *American Association of Petroleum Geologists 1998 annual meeting. AAPG (Tulsa).*

Van de Weerd, A. A., & Armin, R. A. (1992). Origin and evolution of the Tertiary hydrocarbon bearing basins in Kalimatan (Borneo), Indonesia. *American Association of Petroleum Geologists*, 76, 1178–1803.

Van Weering, T. C. E., Nielsen, T., Kenyon, N. H., Akentieva, K., & Kuijpers, A. (1998). Large submarine slides on the NE Faeroe continental margin. In M. S. Stoker, D. Evans, & A. Cramp (Eds.), *Geological processes on continental margins; sedimentation, mass-wasting and stability* (pp. 5–17). *Geological Society of London Special Publications.*

Wilson, M. E. J. (2002). Cenozoic carbonates in Southeast Asia: implications for equatorial carbonate development. *Sedimentary Geology*, 147(3–4), 295–428.

Wilson, M. E. J., Bosence, D. W. J., & Limbong, A. (2000). Tertiary syntectonic carbonate platform development in Indonesia. *Sedimentology*, 47, 395–419.

Wilson, M. E. J., & Moss, S. J. (1999). Cenozoic palaeogeographic evolution of Sulawesi and Borneo. *Palaeogeography, Palaeoclimatology, Palaeoecology*, 145(4), 303–337.

Zampetti, V., Schlager, W., van Konijnenburg, J. H., & Everts, A. J. (2004). Depositional history and origin of porosity in a Miocene carbonate platform of Central Luconia, offshore Sarawak. *Bulletin Geological Society of Malaysia*, in press.